# Cubic law with aperture-length correlation: implications for network scale fluid flow

**Christian Klimczak · Richard A. Schultz · Rishi Parashar · Donald M. Reeves**

**Abstract** Previous studies have computed and modeled fluid flow through fractured rock with the parallel plate approach where the volumetric flow per unit width normal to the direction of flow is proportional to the cubed aperture between the plates, referred to as the traditional cubic law. When combined with the square root relationship of displacement to length scaling of opening-mode fractures, total flow rates through natural opening-mode fractures are found to be proportional to apertures to the fifth power. This new relationship was explored by examining a suite of flow simulations through fracture networks using the discrete fracture network model (DFN). Flow was modeled through fracture networks with the same spatial distribution of fractures for both correlated and uncorrelated fracture length-to-aperture relationships. Results indicate that flow rates are significantly higher for correlated DFNs. Furthermore, the length-to-aperture relations lead to power-law distributions of network hydraulic conductivity which greatly influence equivalent permeability tensor values. These results confirm the importance of the correlated square root relationship of displacement to length scaling for total flow through natural opening-mode fractures and, hence, emphasize the role of these correlations for flow modeling.

**Keywords** Fractured rocks · Fluid flow · Cubic law · Displacement to length scaling · Numerical modeling

Received: 1 May 2009 / Accepted: 15 December 2009
Published online: 19 February 2010



C. Klimczak (✉) · R. A. Schultz
Geomechanics-Rock Fracture Group,
Department of Geological Sciences and Engineering,
University of Nevada,
Mail Stop 172, Reno, NV 89557, USA
e-mail: klimczak@unr.nevada.edu
Tel.: +1-775-8133528
Fax: +1-775-7841833

R. Parashar · D. M. Reeves
Division of Hydrological Sciences,
Desert Research Institute,
2215 Raggio Parkway, Reno, NV 89512, USA

## Introduction

Dilitant fractures in rock (Fig. 1) are the most abundant structures in the brittle part of the Earth's crust. Their size can range from microscopic to regional scales, e.g. microcracks, joints, large-scale joints and joint networks. Wherever bedrock lacks interconnected pore space, as in crystalline or highly consolidated sedimentary rocks, fractures govern the hydraulic properties of these rocks (e.g. Bear et al. 1993; National Research Council 1996). Hence, a study of fractured rock and fracture networks in terms of their hydraulic conductivity is of central importance to the petroleum industry as well as to hydrogeology and geological engineering with implications for contaminant migration through fractured rock masses and petroleum extraction from fractured reservoirs. Accordingly, many studies have put emphasis on the characterization of fractures (e.g. Cowie and Scholz 1992a; Dawers et al. 1993; Dawers and Anders 1995; Rubin 1995; Vermilye and Scholz 1995; Clark and Cox 1996), and modeling of fluid flow through fractures and fracture networks (e.g. Long et al. 1985; Brown 1987; Taylor et al. 1999; Rivard and Delay 2004). So far, however, both fields have mainly been studied independently from each other with relatively few attempts being made to connect the disciplines of fracture mechanics and fracture hydrology with theoretical considerations (de Dreuzy et al. 2001, Baghbanan and Jing 2006; Masihi and King 2007; Neuman 2008) or by matching results of numerical modeling around fracture data from a single borehole (Hartley et al. 2004). In this study, it is shown that fluid flow through fractures can be directly correlated to recently established relationships of fracture scaling that previously have not been exploited by fracture hydrology.

### *Flow through fractures*

In most studies, fluid flow through fractures is conceptualized by using the assumption of laminar flow between parallel plates (Boussinesq 1868; Snow 1965). The parallel-plate solution for the Navier-Stokes equations leads to the commonly used "cubic law" (Lomize 1961; Snow 1965; Louis 1969; Krantz et al. 1979; Tsang and Witherspoon 1981):

$$Q = -\rho g(12\mu)^{-1} b^3 \nabla h, \tag{1}$$


DOI 10.1007/s10040-009-0572-6

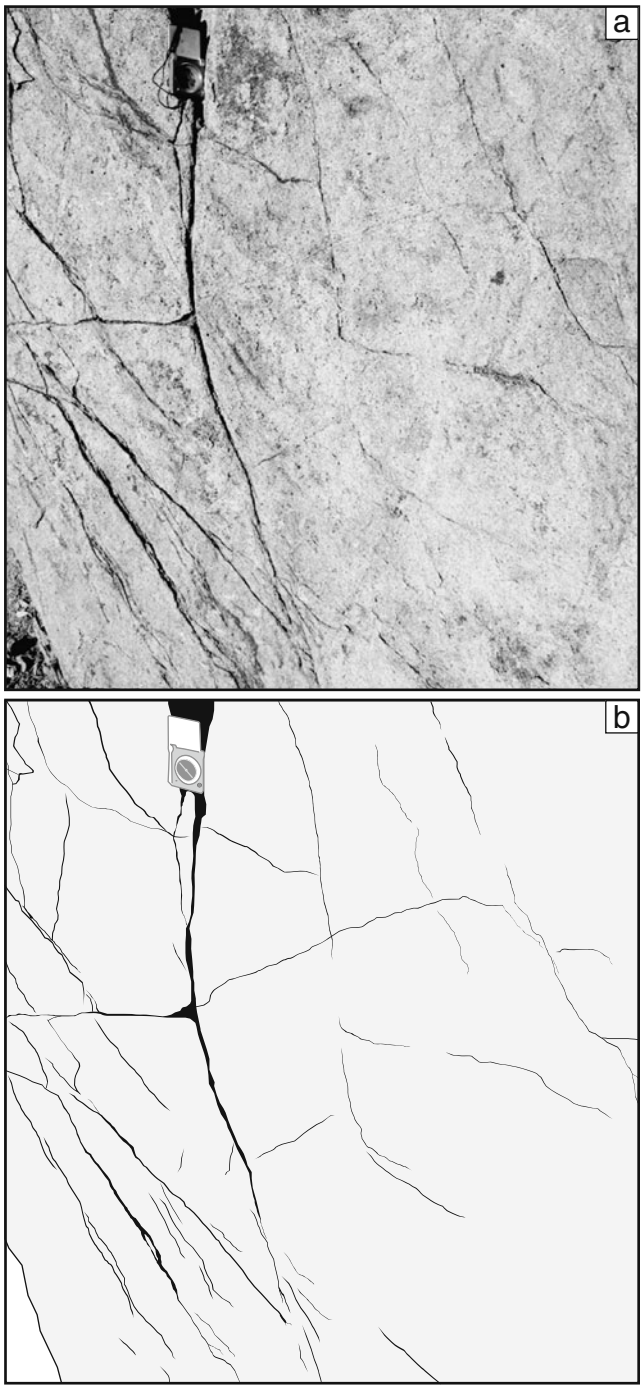


**Fig. 1** Opening-mode fracture network in granitic rocks of the Sierra Nevada batholith near Somerset subdivision, Reno, Nevada. **a** Photograph of the outcrop. Note *compass* for scale. **b** Sketch of same outcrop, *joints traced in black* for emphasis. Longer joints have wider opening displacements

where $Q$, the discharge per unit plate separation, or width, normal to the direction of flow is a function of the cube of the perpendicular distance between the two parallel plates, also referred to as aperture $b$, the fluid density $\rho$, the gravitational acceleration $g$, the fluid viscosity, $\mu$ and the hydraulic gradient, $\nabla h$. The total flow between parallel plates (Fig. 2) results from Eq. (1) by introducing the height, $H$, as:

$$Q = -\rho g(12\mu)^{-1} b^3 \nabla h H. \quad (2)$$

The cubic law accurately describes flow between smooth-walled plates. However, natural fractures are more likely to be rough walled, with walls contacting each other at discrete points (asperities; Gangi 1978; Brown and Scholz 1985; Brown 1987) and lowering total flow. In this case, the equivalent aperture through which fluids can flow, called the hydraulic aperture, is smaller than the actual opening displacement of the fracture or mechanical aperture. The pursuit of correlating mechanical to hydraulic apertures has been met with limited success. Different approaches have attempted to find a representative hydraulic aperture by introducing an empirical relation between mechanical and hydraulic aperture based on hydromechanical coupling experiments (Bandis et al. 1985; Barton et al. 1985), corrections with a friction factor (Witherspoon et al. 1980) due to the tortuosity of the flow path in the fracture (Brown 1987; Cook et al. 1990) or the geometric mean of the aperture distribution (Renshaw 1995).

## Correlation of fracture apertures to fracture lengths

In fracture mechanics, fractures are classified into three displacement modes, i.e. opening-, sliding- and tearing modes, based on the sense of deformation (opening or shearing) in a local coordinate system that is defined by the plane of the fracture (Irwin 1957; Sih 1962; Paris and Sih 1965; Sih and Libowitz 1968; Pollard and Segall 1987). Fracture sets of all three modes have been analyzed in terms of their displacement-length ($D/L$) scaling, a common method in fracture mechanics relating fracture

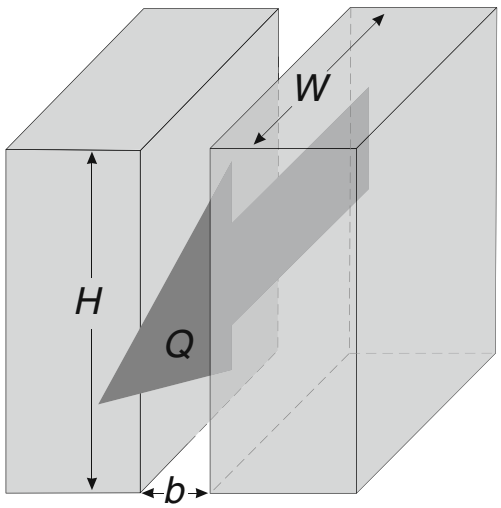


**Fig. 2** Flow ($Q$) between parallel plates with apertures ($b$), plate heights ($H$) and plate lengths ($W$)


DOI 10.1007/s10040-009-0572-6

lengths ($L$) to the corresponding amounts of displacement ($D$). $D/L$ scaling of sliding- (or tearing-) mode discontinuities, i.e. faults, for example, is well documented and understood. Maximum shearing displacements of fault populations are proportional to fault lengths; they scale as a linear function (e.g. Cowie and Scholz 1992a,b; Clark and Cox 1996; Scholz 2002; Schultz et al. 2008a):

$$D_{\max} = \gamma L, \tag{3}$$

where $D_{\max}$ is the maximum (shearing) displacement along the fault, $L$ the length and $\gamma$ a proportionality coefficient related to the rock mechanical properties of the surrounding rock. In Fig. 3 (after Schultz et al. 2008a), the compiled fault data includes a total of 14 fault populations scaling linearly in displacement and length. Values of $\gamma$ range between $10^{-1}$ and $10^{-3}$ (dotted lines) for the entire compilation of faults, with smaller ranges of $\gamma$ for individual fault populations.

Early studies of opening-mode fractures, i.e. joints, veins, and dikes, also suggested a linear relationship between maximum fracture displacements and lengths (Vermilye and Scholz 1995). By linking the general $D/L$ scaling relationship for fractures (Eq. 3) with critical stress intensity factor (fracture toughness) $K_{Ic}$ associated with the growth of joints and other opening-mode fractures, Olson (2003) obtained, instead, a non-linear, square root power-law distribution:

$$D_{\max} = \alpha L^{0.5}, \tag{4}$$

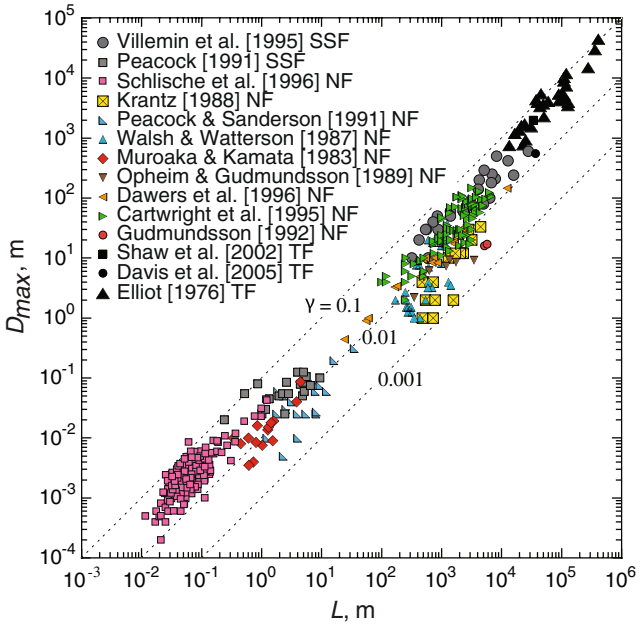


**Fig. 3** Compilation of $D/L$ scaling of faults after Schultz et al. (2008a,b). Normal faults (*NF*), *color symbols*; strike slip faults (*SSF*), *gray symbols*; thrust faults (*TF*), *black symbols*. Lines of constant slope (power-law exponent $n$=1, *dotted lines*) are shown for different $\gamma$

where $\alpha$, the proportionality coefficient:

$$\alpha = \frac{K_{Ic}(1-\nu)^2}{E}\frac{\sqrt{8}}{\sqrt{\pi}} \tag{5}$$

includes the fracture toughness $K_{Ic}$, Poison's ratio $\nu$, and Young's modulus $E$, all material specific constants of the host rock. Olson (2003) further showed that mechanical interaction between closely spaced fractures can lead to variability in scaling exponents depending on the fracture spacing and suggested that exponents greater than $n$=0.5 could result from post-jointing relaxation or other secondary effects.

The exponent of $n$=0.5 is related to a constant fracture toughness, which describes the ability of a rock containing a fracture to resist further fracturing (Olson 2003; Schultz et al. 2008a). This relationship is supported by a total of 10 field datasets composed of up to 46 individual measurements of dikes, veins and joints (Fig. 4), including 7 previously reported fracture sets (Olson 2003; Schultz et al. 2008a; Schultz et al. 2008b) and 3 sets newly acquired for this study. The new data consist of $D_{\max}/L$ measurements of 2 sets of dikes and 1 set of veins from outcrops within the Sierra Nevada batholith (see Appendix 2 for description). All of these datasets are consistent with square-root scaling relationships with exponents ranging from 0.22 to 0.69 and an average of 0.5 (Table 1). The given variability in exponents as reported in the literature and noted here, as well as the intrinsic scatter of measurements (Fig. 4), are explained by several factors including fracture orientation, joint network geometry, mechanical interactions, three-dimensional (3D) shape, and the location along the structure's surface where the displacement was measured.

In the following, the square-root $D/L$ scaling relationship of opening-mode fractures is combined with the cubic law and a relationship for flow between parallel plates with correlated apertures to lengths is derived. Then it is shown that this relationship is important for the prediction of flow rates through fracture networks. Equivalent hydraulic permeability tensors for fracture networks with and without correlated apertures to lengths are computed, compared and interpreted.

## Cubic law with correlated aperture to length

Flow through fractured rock is commonly determined with the cubic law Eq. (1), in which fracture length and aperture are uncorrelated. Previous studies modeled flow rates through fracture networks where apertures were randomly assigned to fracture lengths. Moreover, laboratory experiments on fluid flow through either artificially created fractures (e.g. Watanabe et al. 2008) or natural fractures (e.g. Raven and Gale 1985) involved sampling only a subset of a fracture. Hence, these results were in

 DOI 10.1007/s10040-009-0572-6

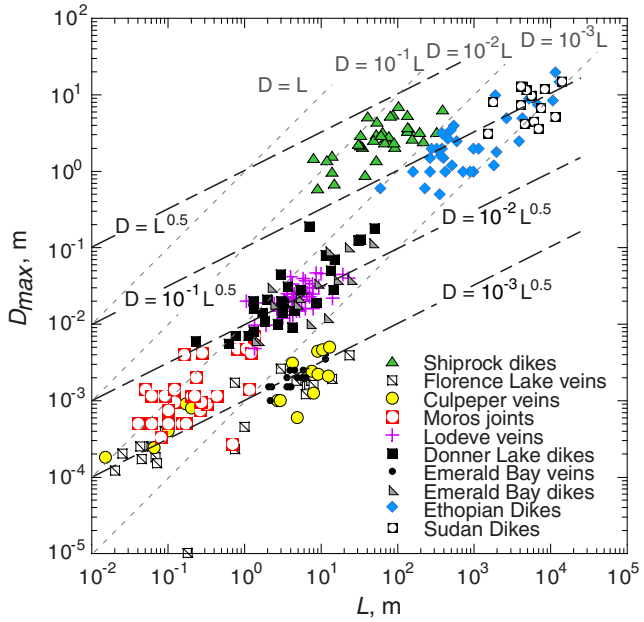


**Fig. 4** Compilation of *D/L* scaling of 10 opening-mode fracture sets. Fracture lengths scale to fracture apertures as power-law functions with exponents $n \sim 0.5$. For reference, several square root functions indicate power-law dependence (*black* dashed lines). For comparison linear functions (*gray* dashed lines) are also shown

accord with the traditional cubic dependence of apertures on flow rates but do not represent total flow through whole natural opening-mode fractures.

Olson (2003) related the maximum opening-mode displacement $D_{\max}$ to the average displacement $D_{\text{avg}}$ as:

$$D_{\text{avg}} = \frac{\pi}{4} D_{\max}. \tag{6}$$

Combining $D_{\max}$ from Eq. (4) with Eq. (6) and solving for $L$, yields

$$L = \frac{16 {D_{\text{avg}}}^2}{(\pi\alpha)^2}. \tag{7}$$

This relationship establishes a correlation between length and the average distance between the walls of a smooth-walled fracture with an elliptical displacement profile. It allows for an elliptical fracture to be modeled as two parallel plates separated by $D_{\text{avg}}$. In this case, $D_{\text{avg}}$ is equal to aperture $b$ in the cubic law (Eqs. 1 and 2). Since the propagation of isolated fractures in homogenous media produce equidimentional crack geometries, called 'penny-shaped' cracks in the fracture mechanics literature (e.g., Lawn 1993 p. 32), where $L$ equals the fracture height $H$ (Jaeger 1969; Timoshenko and Goodier 1970; Jaeger and Cook 1979; Fig. 5), the $D_{\text{avg}}/L$ relationship in Eq. (7) can be substituted for $H$ in the cubic law (Eq. 2) resulting in:

$$Q = -\frac{4\rho g}{3\mu(\pi\alpha)^2} b^5 \nabla h. \tag{8}$$

Total flow through an aperture to length correlated fracture set is proportional to $b^5$, implying a greater non-linearity between flow rate and aperture than predicted by the cubic law. We refer to the previously mentioned form of the cubic law for total flow in a natural fracture with correlated aperture to length as the "quintic law".

The quintic law contains the primary assumptions of the traditional cubic law (Eq. 1) that describes laminar, incompressible fluid flow between two smooth-walled parallel plates separated by distance $b$. Consequently, the same limitations associated with the parallel-plate assumption apply. This pertains in particular to the effect of fracture wall roughness. Despite a lack of agreement of explicit details, all applications accounting for the roughness of the fracture walls (e.g. Bandis et al. 1985; Barton et al. 1985; Witherspoon et al. 1980; Brown 1987; Cook et al. 1990; Renshaw 1995) show that the hydraulic and mechanical apertures of the fracture are related and do not affect the cubic and, hence, quintic exponents (Eqs. 1, 2 and 8).

Using field measurements of apertures and lengths of natural opening-mode fractures (Fig. 4) for flow rate calculations between parallel plates demonstrates that

**Table 1** Values of exponents and proportionality coefficients for opening-mode fracture sets

| Fractures | Exponent | $\alpha$ |
|---|---|---|
| Shiprock dikes | 0.4325 | 0.4435 |
| Florence Lake veins | 0.4916 | 0.0007 |
| Culpeper veins | 0.3941 | 0.0010 |
| Ethiopia dikes | 0.5542 | 0.0527 |
| Moros joints | 0.4789 | 0.0025 |
| Lodève veins | 0.4703 | 0.0102 |
| Sudan dikes | 0.2191 | 1.1645 |
| Emerald Bay veins | 0.5521 | 0.0009 |
| Emerald Bay dikes | 0.6759 | 0.0066 |
| Donnor Pass dikes | 0.6915 | 0.0094 |
| Average | 0.4960 | - |

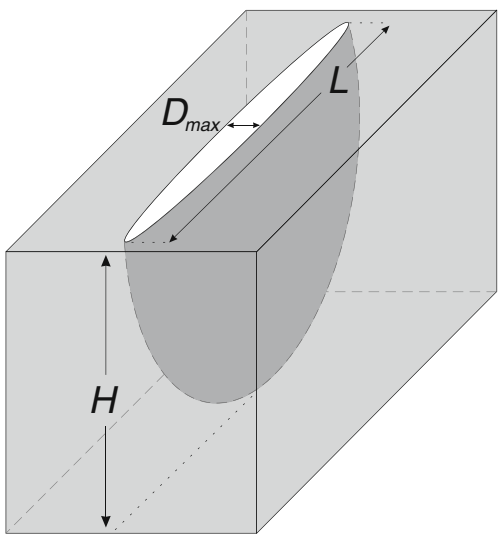


**Fig. 5** 'Penny-shaped' opening-mode fracture model with elliptical opening displacement profile showing fracture length $L$, maximum displacement $D_{max}$ and fracture height, $H$


DOI 10.1007/s10040-009-0572-6

there is indeed a higher non-linearity between total flow through natural opening-mode fractures and aperture (Fig. 6). In this diagram, the dependence of total flow rates on apertures obeys a power law with exponents close to or equal to 5.

The application of the cubic law to faults is not as straightforward, since displacements cannot directly be linked to hydraulic apertures as is possible for joints and other opening-mode fractures such as dikes and veins. Fault displacements can be orders of magnitudes larger than those of opening-mode fractures; however, faults may lack any opening displacements. Therefore, faults can function as barriers or conduits to flow. Despite the fact that faults obey linear *D/L* scaling relationships, their roles in conducting fluid flow depend on several other parameters that cannot easily be generalized. An incorporation of faults into general models for fluid flow is therefore not considered in this study.

Both the mathematical consideration in Eq. (8) as well as the computation of flow rates with data from natural opening-mode fracture sets (Fig. 6) point to a quintic dependence between flow rates and fracture apertures. This indicates that, in a fracture network, the longer fractures with wider apertures conduct higher volumes of fluids, whereas shorter fractures with smaller apertures conduct smaller volumes. In the following, flow is simulated through opening-mode fracture networks with and without aperture-length correlation.

## Numerical simulations

The previous sections describe the power-law relationship between fracture aperture and length for natural fractures,

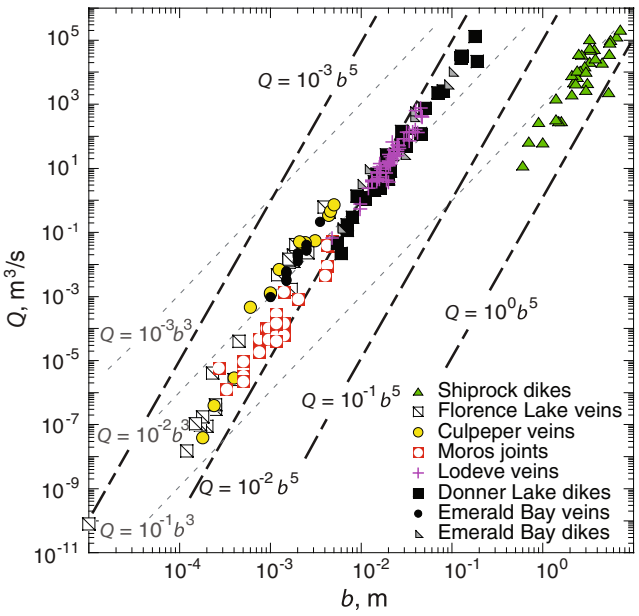


**Fig. 6** Flow rates, derived with cubic law from natural fracture data, are plotted against average apertures of the fractures. Slopes with exponents of 5 (*black dashed lines*) show a better fit than the previously assumed, uncorrelated cubic relation (*gray dashed lines*) and its influence on fluid flow at the single fracture scale. In the following sections, the impact of this power-law dependence on fluid flow at the network scale is investigated.

Flow properties of aperture to length correlated networks are numerically investigated using a two-dimensional (2D) discrete fracture network (DFN) code specifically designed for this study. The DFN code generates random fracture networks according to probability distributions of fracture spacing, length and orientation and values of fracture density. It then computes the hydraulic backbone, the total number of fracture segments capable of conducting flow under the influence of any arbitrary head gradient across the domain boundary, and solves for flow through this backbone. Details on stochastic fracture network generation and solution of flow for given specified boundary conditions will be discussed in the following.

Equivalent permeability tensors ($\overline{\overline{k}}$), based on global network flow through the faces of the DFN, are used as a metric to compare flow through aperture-length correlated networks and classical discrete fracture network simulations where aperture and length are assumed to be uncorrelated. These two cases are referred to as "correlated" and "uncorrelated" networks, respectively. The same spatial distribution of fractures in the backbone structure is used for both correlated and uncorrelated cases. Individual segments of the uncorrelated network are randomly assigned the same hydraulic conductivity ($K$) values computed during the generation of the correlated network. This procedure preserves both the network geometry and underlying $K$ distribution from the correlated network, and, thus, ensures accurate and reliable comparisons between correlated and uncorrelated cases.

Stochastic generation of fracture networks within the model domain involves the addition of fractures with random location, length and orientation until a specified criterion is reached (Table 2). For all network cases, the density criterion is above the percolation threshold and is conducive to backbones that contain multiple domain-spanning interconnected clusters (Fig. 7). The portion of fractures exceeding a given length is modeled according to a power-law dependence on length: $1-F(L) \in L^{-a}$, where $F(L)$ is the cumulative distribution function (CDF) for length $L$, and $a$ is the power-law exponent (Davy 1993; Marrett 1996; Renshaw 1996; Odling 1997; Renshaw 1999; Bonnet et al. 2001) . For this study values for $a$ were chosen to be $a$=1, $a$=2 and $a$=3. If $L \in [L_{min,}\infty)$, then the CDF is given as:

$$F(L) = 1 - L_{\min}^{a} L^{-a}. \tag{9}$$

Differentiating Eq. (9) yields the probability density function (PDF) for length,

$$f(L) = \frac{aL_{\min}^{a}}{L^{a+1}}. \tag{10}$$

Length values described by Eq. (10) are generated in the models by computing $L_{min} U^{-(1/a)}$, where $U$ is a


DOI 10.1007/s10040-009-0572-6

**Table 2** Parameters used for the generation of the fracture networks

| Power-law exponent, $a$ | 1.0 | 2.0 | 3.0 |
|---|---|---|---|
| Fracture density, m/m$^2$ | 0.7 | 1.2 | 2.0 |
| Domain width, m | ≤100 | ≤80 | ≤60 |
| Domain length, m | ≤100 | ≤80 | ≤60 |
| Mean orientation, $\omega$, of set 1 | 0° | 0° | 0° |
| Variation in orientation, $\kappa$, set 1 | 30 | 30 | 30 |
| Probability, set 1 | 50% | 50% | 50% |
| Minimum fracture length, set 1, m | 2 | 2 | 2 |
| Mean orientation, $\omega$, of set 2 | 90° | 90° | 90° |
| Variation in orientation, $\kappa$, set 2 | 30 | 30 | 30 |
| Probability, set 2 | 50% | 50% | 50% |
| Minimum fracture length, set 2, m | 2 | 2 | 2 |

uniform random variable between zero and one. The locations of fracture centers are assumed to be uniformly distributed over the computational domain. The fracture orientations are modeled according to von Mises-Fisher distribution functions which may be thought of as a circular (or spherical in 3D) analogue of the normal distribution. The PDF for von Mises-Fisher distribution for the angle $\theta$ is given as:

$$f(\theta|\omega,\kappa) = \frac{e^{\kappa\cos(\theta-\omega)}}{2\pi I_0(\kappa)} \tag{11}$$

where $I_0(\kappa)$ is the modified Bessel function of order zero. The parameter $\omega$ is the measure of location around which the distribution is clustered and is analogous to the mean in the normal distribution. The parameter $\kappa$ is an inverse measure of the dispersion around a mean orientation, $\omega$, i.e., if $\kappa$ is small, the distribution becomes close to uniform, whereas if $\kappa$ is large, the distribution becomes concentrated about the mean orientation, $\omega$. To generate random variables for the von Mises-Fisher distribution, the algorithm given by Best and Fisher (1979) is used.

The fracture networks each contain two sets of fractures (differing only in their mean orientation, $\omega$) for three length distribution functions with power-law exponent values of 1, 2, and 3, respectively (Table 2). The mean orientations of the fracture sets in all cases are orthogonal according to values of 0° and 90° with $\kappa$ equal to 30 to allow for significant deviation in orientation from the mean. The orthogonal orientation is intended to simplify the computation of the hydraulic conductivity tensor by effectively restricting the non-diagonal components to zero. Fractures are generated until the 2D fracture density satisfies the value given in Table 2. Note that lower values of the power-law exponent leads to the generation of longer fractures (Fig. 8), and consequently a higher degree of connectivity between the fractures. As a result, density values required to establish a hydraulic backbone sufficiently above the percolation threshold are less for lower exponent values (Table 2).

Hydraulic conductivity values for the correlated networks are computed first using Eq. (7) to relate fracture length to average (hydraulic) aperture $b$, and then using the classical cubic law to compute $K$, where $K=\rho g(12\mu)^{-1}b^2$. Note that the simulations in this study are in 2D; hence the quintic relationship described by Eq. (8) does not directly apply since fracture height in the simulations is set to unity. The dependence of fracture length on aperture, given the power-law distribution of fracture length, results in power-law distributions of $K$. Specifically, the distribution of $K$ within the fracture networks is proportional to $K^{-a}$, where $a$ is the fracture length exponent; note that the square root dependence of

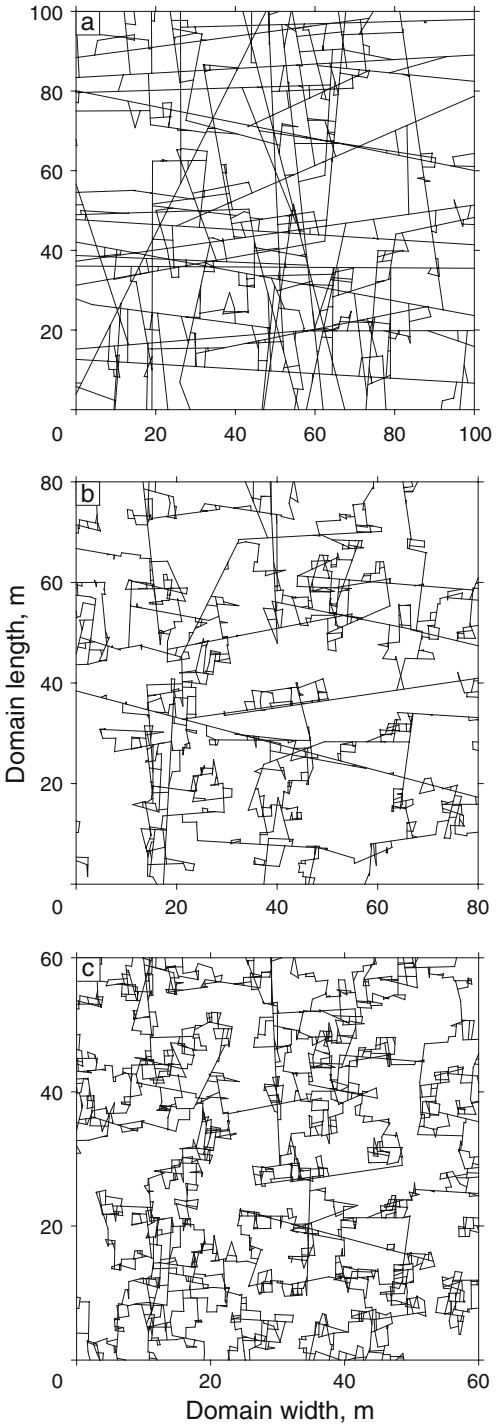


**Fig. 7** Typical hydraulic backbones for power-law length exponents of **a** $a$=1.0, **b** $a$=2.0 and **c** $a$=3.0 and associated parameters (Table 2)


DOI 10.1007/s10040-009-0572-6

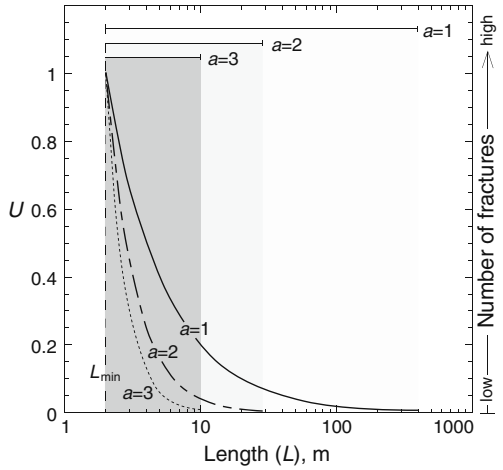


**Fig. 8** Computed length distributions for exponents of $a=1$, $a=2$ and $a=3$ showing the different ranges of fracture lengths for the different exponents

length on aperture and the squared dependence of aperture on $K$ cancel each other. This results in $K$ distributions that become less broad as values of $a$ increase from 1 to 3. This observation could possibly influence the domain size at which a representative elementary volume (REV) is established. Values of $K$ computed from the correlated networks are randomly shuffled and then assigned to individual fracture segments of the uncorrelated network, thereby preserving the distribution of $K$ between the correlated and uncorrelated cases.

Isolated fractures, isolated clusters, and dead-end segments are eliminated next to determine the configuration of the hydraulic backbone. Typical configurations of hydraulic backbone for parameters listed in Table 2 are shown in Fig. 7. As is evident from the backbone, the cases of $a=1$ and $a=3$ are dominated by very long and very short fractures respectively. The case of $a=2$ represents an even mix of longer and shorter fractures. One would expect an increased flow heterogeneity for fracture networks with longer fractures than for the cases with shorter fractures. Hence, the maximum domain width and domain length (Table 2) used in the simulation decreases with increasing $a$.

Instead of computing equivalent $\overline{\overline{k}}$ at a fixed domain size (e.g. Zhang et al. 1996), changes in $\overline{\overline{k}}$ with the scale of the domain are examined to identify the scale at which an REV is established (Kulatilake and Panda 2000; Baghbanan and Jing 2006; Chen et al. 2008). Previous studies were restricted to a few thousand nodes (i.e., fracture intersections) distributed according to either small domain sizes with higher fracture density (Kulatilake and Panda 2000; Min et al. 2004; Baghbanan and Jing 2006; Chen et al. 2008) or larger domains with smaller network density (Zhang et al. 1996). However, the numerical methods employed by the DFN code in this study have dramatically reduced simulation times as compared to previous studies. This allows investigation of both a greater number of domain length scales and statistically equivalent realizations for each network type. Ten domain sizes are considered, starting at 10% of the maximum size and increment in multiples of 10%, for each value of $a$. The net flow rate through the domain is composed of the principal flow rates in the $x$-direction ($q_{xx}$) and $y$-direction ($q_{yy}$), and the cross flow rates ($q_{xy}$ and $q_{yx}$). Suitable head boundary conditions are imposed on the networks (Fig. 9) and flow rate components are computed for all domain sizes by using the techniques of a discrete fracture network (DFN) model as elucidated in Priest (1993). The process is repeated for cases with an uncorrelated permeability field and the corresponding flow rate components are obtained. By assigning mean orthogonal fracture sets with orientations aligned with the principal directions of a Cartesian coordinate system (Table 2), comparable values of flow rates in the principal directions are ensured. The principal and off-diagonal components of $K$ can be determined from the matrix form of Darcy's law (Zhang et al. 1996):

$$\begin{bmatrix} q_{xx} & q_{xy} \\ q_{yx} & q_{yy} \end{bmatrix} = \begin{bmatrix} K_{xx} & K_{xy} \\ K_{yx} & K_{yy} \end{bmatrix} \begin{bmatrix} \nabla H_x & 0 \\ 0 & \nabla H_y \end{bmatrix} \tag{12}$$

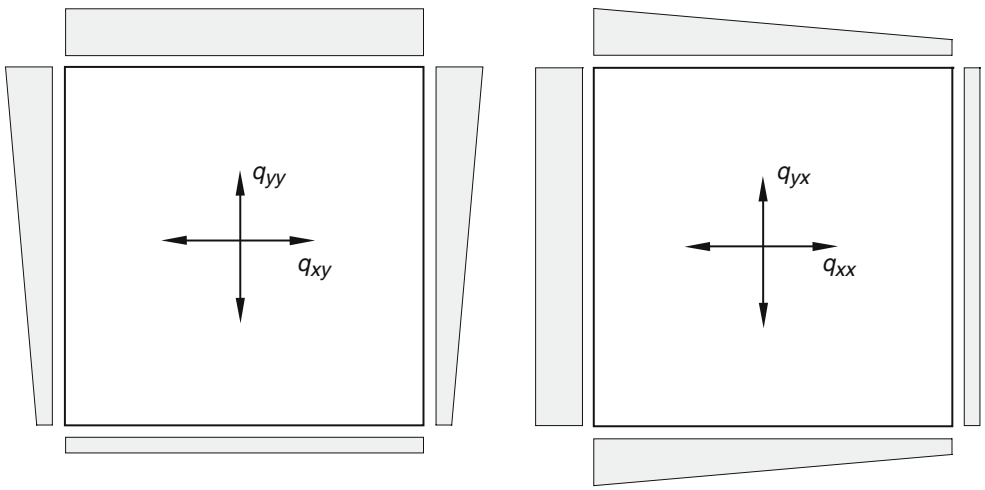


**Fig. 9** Principal flow directions for a 2D domain with linear head boundary conditions shown in the $x$-direction ($q_{xx}$), $y$-direction ($q_{yy}$), and the cross flow directions ($q_{xy}$ and $q_{yx}$)

 DOI 10.1007/s10040-009-0572-6

where $\nabla H_x$ and $\nabla H_y$ are the head gradients in the $x$- and $y$-directions respectively. Components of equivalent $\overline{\overline{k}}$ can easily be computed by inverting Eq. (12). In the simulations, a unit head gradient in both directions for all domain sizes is used, so that the value of the components of flow rate and the components of equivalent $\overline{\overline{k}}$ are numerically equal. Therefore, the four components of hydraulic conductivity tensor are computed for the correlated case for all ten domain sizes and each value of exponent $a$. This process is then repeated for the uncorrelated case. Final values of $\overline{\overline{k}}$ represent the ensemble-average from 100 Monte Carlo simulations. On a computational cluster with 32 CPUs, the efficacy of the code was demonstrated by a simulation time of about 15 min for case with power-law exponent of 1, a simulation time of about 2 h for case with power-law exponent of 2, and a simulation time of about 10 h for case with power-law exponent of 3. The increase in simulation times is caused by the higher fracture densities required to reach a suitable backbone, where the number of unknowns (fracture intersections) within the interior of the DFN for the largest sizes for the above exponents is approximately around 1,200, 2,200 and 4,000, respectively.

## Results and discussion

Information on flow rates calculated from natural fracture data sets (Fig. 6) and the derivation of the quintic law (Eq. 8) both indicated a higher non-linearity between flow rates and fracture apertures. The effects of this quintic relationship were explored by modeling the permeability tensor ($\overline{\overline{k}}$) and an investigation in the establishment of an REV of identical fracture networks with either correlated or uncorrelated apertures to lengths. Due to the correlation of aperture to length and, hence, correlation of the hydraulic conductivity ($K$) to fracture lengths, the $K$-distribution becomes directly linked to the power-law fracture length distribution. Modeling flow through fracture networks is, in this study, therefore based on a power-law $K$ distribution as opposed to more commonly used lognormal distributions.

Results of the numerical simulations indicate that correlated fracture networks of all fracture length distributions have a significantly higher permeability than the uncorrelated networks (Fig. 10). In addition, $\overline{\overline{k}}$ displays a change from an upward trend for fracture length distributions with exponents of $a$=1 to a downward trend for $a$=3. Only for $a$=2 an REV is established in the range of modeled DFN sizes (Fig. 10).

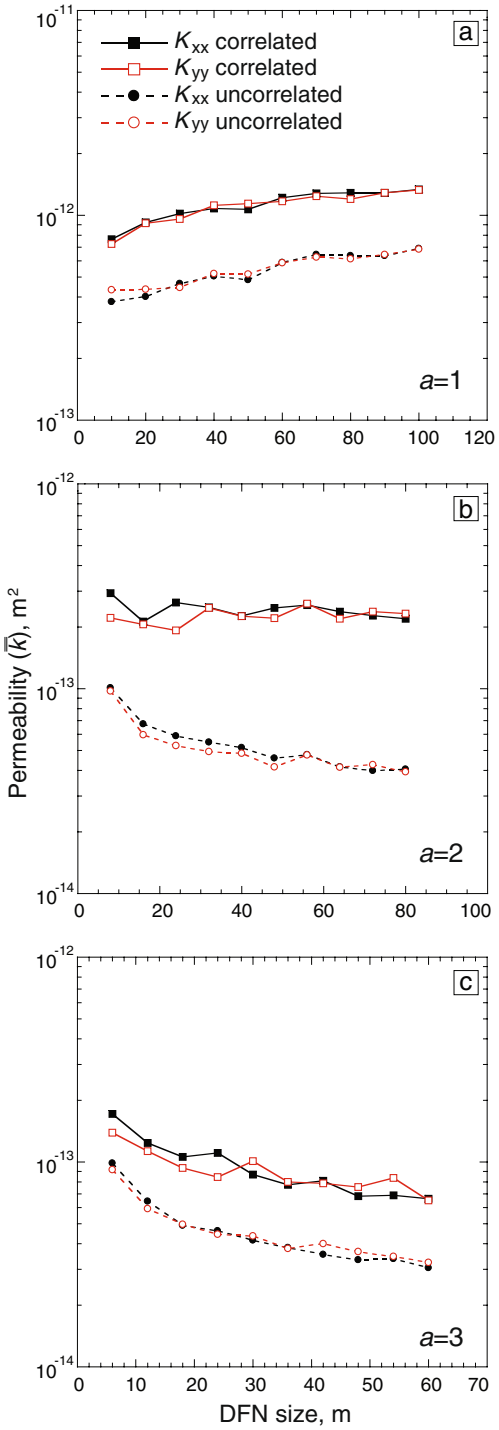


**Fig. 10** Ensemble averaged values for the principal components of $\overline{\overline{k}}$ for correlated and uncorrelated networks. The *black curves* represent $K_{xx}$ and the *red curves* represent $K_{yy}$. *Solid lines* indicate $\overline{\overline{k}}$ for correlated fracture networks and *dashed lines* show $\overline{\overline{k}}$ for the uncorrelated fracture networks, respectively. **a** Values of principal $\overline{\overline{k}}$ components $K_{xx}$ and for $a$=1.0. Note the consistent difference by a factor of about two in principal $\overline{\overline{k}}$ values for the correlated and uncorrelated cases, and the upward trend in principal $\overline{\overline{k}}$ values with DFN size. **b** Values of principal components $K_{xx}$ and $K_{yy}$ for $a$=2.0. Note the consistent difference by a factor of about six in principal $\overline{\overline{k}}$ values for the correlated and uncorrelated cases, and the relatively flat trend in principal $\overline{\overline{k}}$ values with DFN size. **c** Values of principal $\overline{\overline{k}}$ components $K_{xx}$ and $K_{yy}$ for $a$=3.0. Note the consistent difference by a factor of about two in principal $\overline{\overline{k}}$ values for the correlated and uncorrelated cases, and the downward trend in principal $\overline{\overline{k}}$ values with DFN size


DOI 10.1007/s10040-009-0572-6

Differences in principal permeability values between the correlated and uncorrelated cases are a direct result of the proposed correlation. Again, it is emphasized that both cases have the same power-law $K$ distributions. For correlated networks, each fracture gets assigned the appropriate $K$ value according to the square root aperture-to-length relationship. Therefore, the longest fractures have the widest apertures and as a result of that they have the highest conductivities. Hence, they also have the highest impact on the permeability of the fracture network in terms of greatest amount of flow given their role in linking otherwise isolated clusters in the network. For uncorrelated networks, however, this same $K$ distribution is shuffled and randomly assigned to fractures of any length. Consequently, the longer fractures can have low $K$ values, whereas shorter fractures can have high $K$ values. Neither the long fractures with low $K$ values nor the short fractures with possible high $K$ values significantly increase network fluid flow resulting in the lower equivalent permeability values for the uncorrelated fracture networks.

Differences in principal $\overline{\overline{k}}$ values between the correlated and uncorrelated networks are relatively constant (Fig. 10). For length distributions with exponents of $a=1$ and $a=3$, the principal $\overline{\overline{k}}$ values for the correlated networks are more than twice as high when compared to the uncorrelated ones (Fig. 10a,c). Principal $\overline{\overline{k}}$ values for correlated networks with length distributions of $a=2$ are even higher; they differ by a factor of 6 when compared to the principal $\overline{\overline{k}}$ values of uncorrelated networks (Fig. 10)b.

There is an upward trend in permeability tensor values for lower exponents of length distributions, whereas downward trends are present for higher exponents (Fig. 10). In particular, length distribution exponents of $a=1$ lead to $\overline{\overline{k}}$ values that increase with DFN size (Fig. 10)a. For length distribution exponents of $a=1$, the probability of longer fractures in larger DFN sizes is increased (Fig. 8), also resulting in the generation of higher $K$ values. This broadening of the $K$ distribution yields, regardless of the correlation, higher permeability values with increasing domain size. Here, the impact of the longer fractures is maximized with the increase in size of the fracture network.

In contrast, fracture networks with length distribution exponents of $a=3$ produce values of $\overline{\overline{k}}$ that decrease with DFN size (Fig. 10c) for both correlated and uncorrelated DFN. As apparent in Fig. 8 the downward trend of the fracture length distribution is rather steep, indicating that shorter fractures occur far more often than longer fractures. The probability of shorter fractures less than the size of the DFN is much greater than for longer fractures causing an increasing ratio of short to long fractures. Consequently, the probability of lower $K$-values is also increased, minimizing the impact of the longer fractures with increasing DFN size and, therefore, reducing the permeability for larger domain sizes.

A transitional behavior of the $\overline{\overline{k}}$ trends of the curve exists for fracture length distributions around $a=2$. Whereas the uncorrelated DFN simulations result in a downward curve, similar to curves for $a=3$, the $\overline{\overline{k}}$ tensor for the correlated case is almost constant for all DFN sizes (Fig. 10b). For $a=2$, the fracture length distribution is intermediate (Fig. 8), with an even mixture of long and short fractures exists. This even mixture also controls the $K$ distribution and most likely explains why the downward and upward trends of the tensor are effectively balanced with changes in DFN size.

As mentioned previously, the power-law distributions used to compute $K$ values for individual fractures are directly linked to fracture length. Accordingly, the heterogeneity in the $K$ distribution decreases as the length distribution exponent increases from $a=1$ to $a=3$. Based on this quality, one would expect an REV to be established in the order of less heterogeneity. However, results of this study show that an REV only exists for networks with fracture-length distribution exponents of $a=2$ where an REV is established around a DFN size of 50 m (Fig. 10b). In contrast, values of the $\overline{\overline{k}}$ tensor for networks with length distribution exponents of $a=1$ and $a=3$ display an ongoing upward trend or downward trend respectively (Fig. 10a,c). This shows that there is no REV established within the modeled range of DFN sizes. In addition, the ongoing upward ($a=1$) and downward ($a=3$) trends suggest that these networks may not satisfy REV conditions within scales at which DFN are computationally feasible.

The lack of the formation of an REV is closely related to the length distribution. Backbones with length distributions where the exponent is low ($a=1$) are dominated by long fractures (Fig. 7a), where the longest fractures are constantly truncated by the domain size. As DFN size increases, fractures become longer and can further promote fluid flow through enhanced connectivity. The opposite is true for fracture networks with length distributions where exponents are high ($a=3$). Here, the backbone is dominated by short fractures (Fig. 7c). The importance of longer domain spanning fractures is constantly diminished with increasing domain size resulting in the observed decrease of permeability for increasing network sizes. Again, for networks with fracture length distributions around $a=2$, the even mixture of short and long fractures promotes the establishment of an REV.

De Dreuzy et al. (2002) previously investigated the influence of a power-law aperture distribution on the permeability of fracture networks. Based on the use of a power-law length distribution for their modeling experiments and linear aperture to length scaling relationships (e.g. Vermilye and Scholz 1995), they concluded that the aperture distribution must also obey a power law. When combining their proposed aperture distribution with the cubic law, they also obtained a power-law permeability distribution for their fracture networks. Results show that, for low exponents, flow is channeled independent of system size, whereas higher exponents cause the flow to be much more distributed over the fracture network. Observations by de Dreuzy et al. (2002) are, in general, consistent with this study. However, our simulations show an intensification of the observed effects with increasing scale (Fig. 10). Secondly, our simulations are consistent

 DOI 10.1007/s10040-009-0572-6

with more recently determined square root aperture to length scaling (Olson 2003), where each individual fracture length is correlated to its appropriate aperture so that power-law distributions of $K$ are proportional to $K^{-a}$ with $a$ being the fracture length exponent. Our results emphasize the importance of the choice of aperture to length scaling function (i.e., Eq. 4).

Renshaw (1999) compiled estimates of power-law exponents and obtained a mean exponent of $a$=1.8 with a standard deviation of 0.4. This suggests that fracture-length distribution exponents for the majority of natural fractures should range between 1.4 and 2.2. For this range results, of this study ($a$=2) exhibit a difference in principal $\overline{\overline{k}}$ values between correlated and uncorrelated networks of a factor of 6. Hence, modeling flow through fracture networks with correlated fracture length to aperture, as observed in nature, indicates that volumetric flow rates are likely underestimated with conventional modeling approaches where fracture length and permeability are uncorrelated. Higher volumetric flow rates also suggest that volume estimates of jointed petroleum and groundwater reservoirs are higher than previously assumed. Furthermore, the correlation between length and aperture of fracture sets shows that inverse measures of hydraulic apertures (e.g. Watanabe et al. 2008) were overestimated with the traditional cubic law. Obtaining hydraulic apertures from measured flow rates using the quintic relationship would yield lower values.

Fracture sets with correlated aperture to length and a fracture length distribution exponents of $a$=2 most closely reflect flow characteristics of natural fracture sets in this study. For this case, results show relatively constant $\overline{\overline{k}}$ values throughout all DFN sizes. However, simulations here only investigated DFN with fracture densities slightly above the percolation threshold. Further studies in this range of distribution exponents with different fracture densities could provide a better understanding of the permeability for natural fracture sets.

## Conclusions

Given the square root correlation of fracture apertures to lengths with flow between parallel plates, total flow rates through natural opening-mode fractures are shown to be proportional to apertures to the fifth power. The correlation also demonstrates that the hydraulic conductivity of the network is directly related to the power-law length distribution applied to the fracture sets. For DFN flow modeling, this quintic law is reflected in usage of a power-law $K$ distribution, where each fracture of a network was assigned the appropriate $K$ value. Results were compared to networks with the same spatial distribution of fractures but $K$ values were arbitrarily assigned to fractures. Results indicate that correlated fracture networks have up to 6 times higher principal $\overline{\overline{k}}$ values than uncorrelated networks. In addition, results show that the power-law $K$ distribution exerts a significant impact on the tensor curve and the associated establishment of an REV. Curves for networks with length distributions where the exponents are either low ($a$=1) or high ($a$=3) have ongoing upward or downward trends respectively and, within the tested range, the REV is not established. The intermediate example for networks with an exponent of the length distribution of $a$=2 shows relatively constant values for the $\overline{\overline{k}}$ tensor throughout all DFN sizes, also an REV is established.

Results of the simulations are consistent with observations and calculations of flow rates through natural fractures and they point out the importance of the square root correlation. Consequently, these results indicate that the quintic law should be taken into account for the computation and simulation of flow rates through natural opening-mode fracture sets and networks.

**Acknowledgements** We thank J. Johnson, an anonymous referee, and the Associate Editor for their detailed and thoughtful comments that sharpened the final paper. This work was supported by a grant from NASA's Planetary Geology and Geophysics Program to R.A. S.; R.P. and D.M.R. were partially supported by funding provided by the Desert Research Institute.

## Appendix 1: Notation

| | |
|---|---|
| $a$ | Fracture length distribution exponent |
| $\alpha$ | Proportionality coefficient (opening-mode fractures), $m^{1/2}$ |
| $b$ | Aperture, m |
| $D$ | Displacement, m |
| $D_{avg}$ | Average opening displacement, m |
| $D_{max}$ | Maximum opening displacement, m |
| $\Delta\ \sigma_I$ | Opening-mode driving stress, Pa |
| $E$ | Young's modulus, Pa |
| $\theta$ | Fracture orientation |
| $g$ | Acceleration of gravity, $m/s^2$ |
| $\gamma$ | Proportionality coefficient (faults) |
| $H$ | Height of parallel plates, fracture height, m |
| $\nabla h$ | Hydraulic head gradient |
| $\nabla H_x$ | Head gradient in $x$-direction |
| $\nabla H_y$ | Head gradient in $y$-direction |
| $I_0(\kappa)$ | Modified Bessel function of order zero |
| $K_{Ic}$ | Fracture toughness, MPa $m^{1/2}$ |
| $\underline{K}$ | Hydraulic conductivity, m/s |
| $\overline{\overline{k}}$ | Permeability tensor, $m^2$ |
| $K_{xx}$ | Principal direction of permeability tensor, $m^2$ |
| $K_{xy}$ | Principal direction of permeability tensor, $m^2$ |
| $K_{yx}$ | Cross direction of permeability tensor, $m^2$ |
| $K_{yy}$ | Cross direction of permeability tensor, $m^2$ |
| $\kappa$ | Variation in fracture orientation |
| $L$ | Fracture length, m |
| $L_{min}$ | Minimum fracture length, m |
| $\mu$ | Viscosity, Pa s |
| $Q$ | Volumetric discharge, $m^3/s$ |
| $q_{xx}$ | Principal direction of specific discharge, m/s |
| $q_{yx}$ | Cross direction of specific discharge, m/s |
| $q_{yx}$ | Cross direction of specific discharge, m/s |
| $q_{yy}$ | Principal direction of specific discharge, m/s |

 DOI 10.1007/s10040-009-0572-6

$\rho$ Fluid density, kg/m$^3$
$U$ Random variable for fracture length computation
$V_f$ Fracture volume, m$^3$
$\nu$ Poisson's ratio
$W$ Length of parallel plates
$\omega$ Mean fracture orientation

## Appendix 2

The fault datasets presented in Fig. 3 are taken from Schultz et al. (2008a) and references therein. The opening-mode fracture datasets in Fig. 4 consist of seven previously reported datasets from Olson (2003) and Schultz et al. (2008a, b). Three newly acquired datasets were measured in outcrops of the Sierra Nevada batholith around Lake Tahoe, CA.

A set of NW/SE striking vertical dikes was carefully measured in terms of their length and opening displacement in exposures of glacially polished Mesozoic granitoids of the Donner Summit Pluton, near Donner Pass, CA. Two types of dikes were observed. Simple dikes comprise the majority of dikes in this region and are of granodioritic composition. The second type of dikes, referred to as complex dikes consist of two phases, an outer pegmatitic phase and an inner phase of a more mafic composition (Ward 1993). This dataset consists of a total of 28 $D/L$ measurements ranging from 1.13 to 50.5m in length.

Glacially polished granitoids are also present west of Emerald Bay State Park, CA. Here, a set of E/W striking dikes of pegmatitic composition and another set of steeply NE\SW striking quartz-filled veins was measured between Cascade Lake and Granite Lake. Both sets each include 14 individual measurements of fracture length and opening displacement. Measured dike lengths range between 1.38 and 48m. Measured veins have lengths between 2.06 and 11.42m. Measurements were taken with a 30-m steel tape, displacements and lengths have measurement uncertainties of ±0.5 and ±10mm, respectively.

## References


Baghbanan A, Jing L (2006) Hydraulic properties of fractured rock masses with correlated fracture length and aperture. Int J Rock Mech Min Sci 44:704–719

Bandis SC, Makurat A, Vik G (1985) Predicted and measured hydraulic conductivity of rock joints. Proceedings of the International Symposium on Fundamentals of Rock Joints, Bjorkliden, Sweden, 15–20 September, pp 269–280

Barton NR, Bandis SC, Bakhtar K (1985) Strength, deformation and conductivity coupling of rock joints. Int J Rock Min Sci Geomech Abstr 22(3):121–140

Bear J, Tsang CF, de Marsily G (1993) Flow and contaminant transport in fractured rock. Academic, San Diego, CA

Best DJ, Fisher NI (1979) Efficient simulation of the von Mises distribution. Appl Stat 28(2):152–157

Bonnet E, Bour O, Odling NE, Davy P, Main I, Cowie P, Berkowitz B (2001) Scaling of fracture systems in geologic media. Rev Geophys 39(3):347–383

Boussinesq J (1868) Memoire sur l'influence des frottements dans les mouvements reguliers des fluids [Thesis about the influence of friction within the steady flow of fluids]. J Math Pures Appl 13:377–424

Brown SR (1987) Fluid flow through rock joints: the effect of surface roughness. J Geophys Res 92:1337–1347

Brown SR, Scholz CH (1985) The closure of random elastic surfaces in contact. J Geophys Res 90:5531–5545

Chen SH, Feng XM, Isam S (2008) Numerical estimation of REV and permeability tensor for fractured rock masses by composite element method. Int J Numer Anal Meth Geomech 32:1459–1477

Clark RM, Cox SJD (1996) A modern regression approach to determining fault displacement-length scaling relationship. J Struct Geol 18:147–152

Cook AM, Myer LR, Cook NGW, Doyle FM (1990) The effect of tortuosity on flow through a natural fracture. In: Hustrulid WA, Johnson WA (ed) Rock mechanics contributions and challenges, Proceedings of the 31st US Symposium on Rock Mechanics. Golden, CO, June 1990

Cowie PA, Scholz CH (1992a) Physical explanation for the displacement-length relationship of faults using a post-yield fracture mechanics model. J Struct Geol 14:1133–1148

Cowie PA, Scholz CH (1992b) Displacement-length scaling relationship for faults: data synthesis and discussion. J Struct Geol 14:1149–1156

Davy P (1993) On the frequency-length distribution of the San Andreas fault system. J Geophys Res 98:12141–12151

Dawers NH, Anders MH (1995) Displacement-length scaling and fault linkage. J Struct Geol 17:607–614

Dawers NH, Anders MH, Scholz CH (1993) Growth of normal faults: displacement-length scaling. Geology 21:1107–1110

De Dreuzy J-R, Davy P, Bour O (2001) Hydraulic properties of two-dimensional random fracture networks following a power law length distribution 2: permeability networks based on lognormal distribution of apertures. Water Resour Res 37:2079–2095

Dreuzy D, Davy P, Bour O (2002) Hydraulic properties of two-dimensional fracture networks following power law distributions of length and aperture. Water Resour Res 38, W06412. doi:10.1029/2001WR001009

Gangi AF (1978) Variation of whole and fractured porous rock permeability with confining pressure. Int J Rock Min Sci Geomech Abstr 15:249–257

Hartley L, Cox L, Holton D, Hunter F, Joyce S, Gylling B, Lindgren M (2004) Groundwater flow and radionuclide transport modelling using CONNECTFLOW in support of the SR Can assessment. SKB Rapport R-04-61, Svensk Kärnbränslehantering AB. Swedish Nuclear Fuel and Waste Management Co, Stockholm

Irwin GR (1957) Analysis of stresses and strains near the end of a crack. J Appl Mech 24:361–369

Jaeger JC (1969) Elasticity, fracture and flow: with engineering and geological applications. Chapman and Hall, London

Jaeger JC, Cook NGW (1979) Fundamentals of rock mechanics. Chapman and Hall, London

Krantz RE, Frankel AD, Engelder T, Scholz CH (1979) The permeability of whole and jointed Barre granite. Int J Rock Min Sci Geomech Abstr 16:225–234

Kulatilake PHSW, Panda B (2000) Effect of block size and joint geometry on jointed rock hydraulics and REV. J Engrg Mech 126(8):850–858

Lawn B (1993) Fracture of brittle solids. Cambridge University Press, Cambridge

Lomize GM (1961) Filtrarsiia v Treshchinovatykh Porod [Water flow in jointed rock]. Gosenergoizdat, Moscow

Long JCS, Gilmour P, Witherspoon PA (1985) A model for steady fluid flow in random three-dimensional networks of disc-shaped fractures. Water Resour Res 21:1105–1115

Louis CA (1969) A study of groundwater flow in jointed rock and its influence of the stability of rock masses. Rock Mechanics Research Report 10. Imperial College, London

Marrett R (1996) Aggregate properties of fracture populations. J Struct Geol 18:169–178

Masihi M, King PR (2007) A correlated fracture network: modeling and percolation properties. Water Resour Res 43, W07439. doi:10.29/2006WR005331

Min KB, Jing L, Stephansson O (2004) Determining the equivalent permeability tensor for fractured rock masses using a stochastic REV approach: method and application to the field data from Sellafield, UK. Hydrogeol J 12:497–510

Neuman SP (2008) Multiscale relationships between fracture length, aperture, density and permeability. Geophys Res Lett 35, L22402. doi:10.1029/2008GL035622

National Research Council (1996) Rock fractures and fluid flow: contemporary understanding and applications. National Academy Press, Washington, DC

Odling NE (1997) Scaling and connectivity of joint systems in sandstones from western Norway. J Struct Geol 19:1257–1271

Olson JE (2003) Sublinear scaling of fracture aperture versus length: an exception or the rule? J Geophys Res 108(B9), 2413. doi:10.1029/2001JB000419

Paris PC, Sih GC (1965) Stress analysis of cracks. In: Fracture toughness testing and its applications. Special Technical Publication, vol. 381, American Society for Testing and Materials, West Conshohocken, PA, pp 30–83

Pollard DD, Segall P (1987) Theoretical displacements and stresses near fractures in rock: with applications to faults, joint, veins, dikes and solution surfaces. In: Atkinson BK (ed) Fracture mechanics of rock. Academic Press, San Diego, CA

Priest SD (1993) Discontinuity analysis of rock engineering. Chapman and Hall, London

Raven KG, Gale JE (1985) Water flow in a natural rock fracture as a function of stress and sample size. Int J Rock Mech Min Sci Geomech Abstr 22(4):251–261

Renshaw CE (1995) On the relationship between mechanical and hydraulic apertures in rough-walled fractures. J Geophys Res 100:24629–24636

Renshaw CE (1996) Influence of subcritical fracture growth on the connectivity of fracture networks. Water Resour Res 32 (6):1519–1530

Renshaw CE (1999) Connectivity of joint networks with power law length distributions. Water Resour Res 35(9):2661–2670

Rivard C, Delay F (2004) Simulations of solute transport in fractured porous media using 2D percolation networks with uncorrelated hydraulic conductivity fields. Hydrogeol J 12:613–627

Rubin AM (1995) Propagation of magma-filled cracks. Annu Rev Earth Planet Sci 23:287–336

Scholz CH (2002) The mechanics of earthquakes and faulting. Cambridge Univ Press, Cambridge

Schultz RA, Soliva R, Fossen H, Okubo CH, Reeves DM (2008a) Dependence of displacement-length scaling relations for fractures and deformation bands on the volumetric changes across them. J Struct Geol 30:1405–1411

Schultz RA, Mège D, Diot H (2008b) Emplacement conditions of igneous dikes in Ethiopian Traps. J Volc Geotherm Res 178 (4):683–692

Sih GC (1962) On singular character of thermal stresses near a crack tip. J Appl Mech 29:587

Sih GC, Libowitz H (1968) Fracture. Academic, New York

Snow DT (1965) A parallel plate model of fractured permeable media. PhD Thesis Univ. of Calif., Berkeley, USA

Taylor WL, Pollard DD, Aydin A (1999) Fluid flow in discrete joint sets: field observations and numerical simulations. J Geophys Res 104:28983–29006

Timoshenko SP, Goodier JN (1970) Theory of elasticity. McGraw-Hill, New York

Tsang YW, Witherspoon PA (1981) Hydromechanical behavior of a deformable rock fracture subject to normal stress. J Geophys Res 86:9287–9298

Vermilye JM, Scholz CH (1995) Relation between vein length and aperture. J Struct Geol 17:423–434

Ward KA (1993) Dike emplacement and deformation in the Donner Summit pluton, central Sierra Nevada, California. MSc Thesis, Univ. of Nev., USA

Watanabe N, Hirano N, Tsuchia N (2008) Determination of aperture structure and fluid flow in a rock fracture by high-resolution numerical modeling on the basis of a flow-through experiment under confining pressure. Water Resour Res 44, W06412. doi:10.1029/2006WR005411

Witherspoon PA, Wang JSY, Iwai K, Gale JE (1980) Validity of cubic law for fluid flow in a deformable rock fracture. Water Resour Res 16:1016–1024

Zhang X, Sanderson DJ, Harkness RM, Last NC (1996) Evaluation of the 2-D permeability tensor for fractured rock masses. Int J Rock Mech Min Sci Geomech Abstr 33(1):17–37